Transfer and breakup processes in reactions of 11- and 17-MeV/nucleon ^{20}Ne + ^{197}Au

S. Wald,* S. B. Gazes, C. R. Albiston, Y. Chan, B. G. Harvey, M. J. Murphy,† I. Tserruya,* and R. G. Stokstad

Nuclear Science Division, Lawrence Berkeley Laboratory, University of California, Berkeley, California 94720

P. J. Countryman and K. Van Bibber

High Energy Physics Laboratory and Department of Physics, Stanford University, Stanford, California 94305

H. Homeyer

*Hahn-Meitner-Institut für Kernforschung Berlin, Bereich Kern- und Strahlenphysik,
D-1000 Berlin-39, Federal Republic of Germany*

(Received 5 April 1985)

The mechanisms of transfer and breakup in heavy-ion-induced reactions have been studied for the ^{20}Ne + ^{197}Au system at bombarding energies of 220 and 341 MeV. A 4π detector was used to separate reactions leading to the production of projectilelike fragments into components having either two charged bodies in the final state (transfer) or three or more charged fragments (breakup). For both components, angular distributions, energy spectra, and production cross sections are shown for projectile fragments of $Z = 3-9$. The ratio of transfer to inclusive yields initially drops steeply with decreasing ejectile charge, leveling off for $Z \leq 7$. The lower bounds on this ratio are $\simeq 60\%$ and $\simeq 30\%$ at 220 and 341 MeV, respectively. At 341 MeV, the trends in the central moments (mean, width, and skewness) of the ejectile energy spectra, as a function of Z, are similar for transfer and breakup. The primary ejectile yields are deduced from the breakup and transfer cross sections, and comparisons are made with the predictions of various models. The relatively large probabilities for primary ejectiles to be produced in charged-particle-bound states, observed for all Z and at both 220 and 341 MeV, indicate that, on average, most of the excitation energy resides in the heavy, targetlike fragment.

I. INTRODUCTION

The measurement of transfer processes in heavy-ion-induced reactions has long been used as a testing ground for various theories of heavy-ion reaction mechanisms. At bombarding energies near the Coulomb barrier, macroscopic and microscopic models have generally assumed that all nuclear interactions proceed via one-body processes.[1,2] At higher-energies, however, nucleon-nucleon scattering should become increasingly important.[3] A transition might then be expected to occur as the velocity of the colliding nuclei approaches, and then exceeds, the velocity of sound in nuclear matter ($\simeq 15$ MeV/nucleon) or the intrinsic Fermi velocity ($\simeq 35$ MeV/nucleon). For this reason, a great emphasis has been placed recently upon understanding the processes associated with intermediate-energy reactions in the 10–100 MeV/nucleon regime.[4]

It now appears that the region 10–20 MeV/nucleon witnesses the onset of a variety of different processes. Some of the associated names are preequilibrium emission,[5] incomplete fusion,[6] massive transfer,[7] and projectile breakup.[8–10] Thus, it has become increasingly obvious that experiments must be more selective. Since inclusive measurements, by their very nature, sum over all possible reaction mechanisms, they lack the very selectivity that this energy regime requires.

The problem of selectivity has been addressed in different ways. One approach, utilized by the Hahn-Meitner-Institut (HMI) group,[11] has involved the use of a 4π neutron detector. The number of neutrons emitted in coincidence with a projectilelike fragment is used as a measure of the amount of kinetic energy converted into target excitation energy. This leads to a decomposition of the yield into breakup (small target excitation) and transfer (large target excitation).

Another approach, involving the detection of characteristic K x rays emitted by the targetlike recoil, has been used by the Kernfysisch Versneller Instituut (KVI) group.[12] Here, the focus is on measuring the amount of charge (rather than excitation energy) that is transferred to the target by the projectile. A problem with this technique lies in its inability to detect the charge lost through sequential target decay.

At LBL, a streamer chamber has been used[13] to identify two- and three- (or more) charged-body reactions. In this case, the emission of all charged fragments within a 4π solid angle is clearly delineated by the corresponding tracks. Furthermore, the angular information allows one to assess the relative importance of sequential target decay. The technique does suffer from low count rates as well as the difficulty of extracting all the information contained in the event images. As a result, counting statistics are poor, and only the strongest exit channels can be investigated.

We have constructed a device, the Plastic Box,[14] that is designed to incorporate most of the detection properties of the streamer chamber, but with a much improved data ac-

quisition capability. With the Plastic Box, as with the streamer chamber, it is possible to determine whether a projectilelike fragment detected in a counter telescope (and characterized by charge Z, energy E, and angle θ) is accompanied by one or more charged particles—a breakup reaction—or by none—a transfer reaction. (The targetlike fragment is stopped either in the target or in the Mylar covering the scintillators.) Thus, measured Z, E, and θ distributions of projectilelike fragments can be decomposed into distributions corresponding to each of these two reaction mechanisms.

Within this framework, we analyze the charge, energy, and angular distributions for projectilelike fragments produced in reactions of 11- and 17-MeV/nucleon ^{20}Ne with ^{197}Au. In Sec. II, the Plastic Box is described and details of the experimental technique are given. The results of measurements are presented in Sec. III. In Sec. IV, comparisons are made between reconstructed primary yields and model predictions. The observed ejectile energy spectra are considered in Sec. V. Finally, our results and conclusions are summarized in Sec. VI.

II. EXPERIMENTAL TECHNIQUE

The experiments were performed at the 88-inch cyclotron at Lawrence Berkeley Laboratory. Beams of 220- and 341-MeV ^{20}Ne (charge states 6^+ and 7^+, respectively) were used to bombard self-supporting targets of ^{197}Au (5.3-mg/cm^2 areal density). Beam intensity was typically 1–2 electric nA and was monitored by a Faraday cup placed $\simeq 2$ m from the target. The integrated current was used to normalize the data and provide absolute cross sections.

The configuration of the detectors, as arranged in the

LBL-Krakow 60-inch scattering chamber, is illustrated schematically in Fig. 1. Projectilelike fragments were detected in two triple-element silicon surface-barrier telescopes. Each telescope consisted of two transmission detectors (40 and 100 μm) to measure energy loss, and a thick ($\simeq$5 mm) detector to measure the total energy of the most penetrating fragments. Both telescopes were mounted on a movable arm, with a fixed relative angle of 5°. The solid angles subtended were 0.28 and 0.43 msr. Measurements were made over the angular range of 8°–21°.

The array of plastic scintillators, arranged in a cube centered on the target, consists of 20 cm×20 cm×1 mm sheets of NE-102, each individually coupled on one edge via adiabatic light guides to an RCA 8850 or 8575 photomultiplier tube. In order to provide shielding from ambient light and improve transmission of the scintillation, all scintillators were wrapped in 6.4 μm aluminized Mylar. Though of negligible thickness for light particles, the Mylar prevents the detection of target-associated evaporation residues or fission fragments.

Each of the six walls is made up of two parallel scintillator sheets in order to make corrections for the detection of neutral particles. A typical plot of light output of inner wall (A) versus outer wall (B) is shown in Fig. 2. A region in which only the outer wall fired is clearly discerned and represents the scintillator response to neutrons and gamma rays. By using "ΔE" and "E" scintillators of equal thickness, it is possible to determine directly the number of neutral particles detected by the inner wall. (This is possible due to the low absolute neutron efficiency of a 1-mm-thick plastic sheet.) In this way, average contributions from neutral particles can be subtracted from those events corresponding to charged particles stopping in the inner scintillator. These corrections were found to be relatively small.

The elements of wall 3 have a small hole to allow the beam to enter the box. Similarly, the beam emerged through an opening in wall 1. This opening was in the

The Plastic Box –
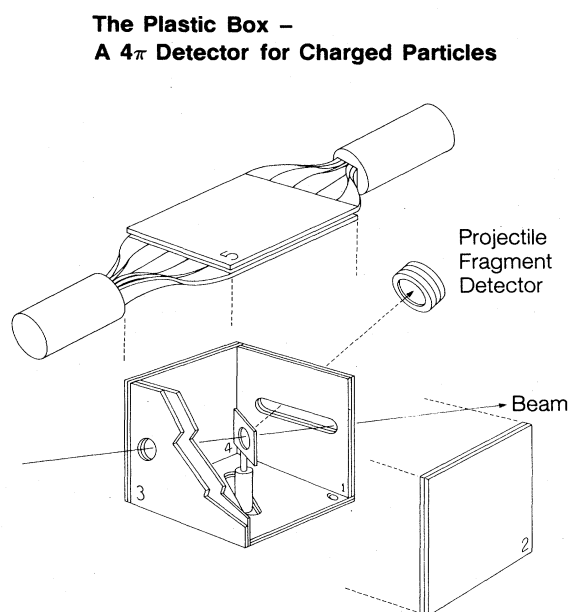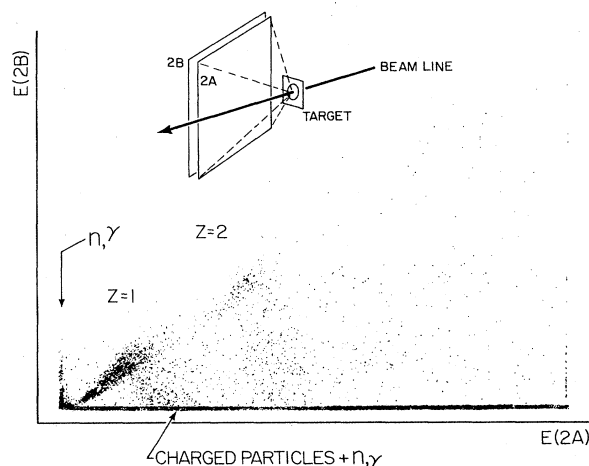**A 4π Detector for Charged Particles**

FIG. 1. The detector configuration is illustrated, including the relative positions of the target, Plastic Box, and one of the telescopes. The wall numbers used in the text are indicated in the figure.

FIG. 2. The pulse heights of inner wall (A) versus outer wall (B) are plotted for inclusive events in wall number 2. Contributions from charged particles as well as neutral events are indicated.

form of a horizontal slot, through which the solid-state telescopes could view the target. The extent of this slot restricted the telescopes to a maximum angle of 21° from the beam axis. Part of the solid angle lost due to this slot was regained by using another wall of plastic scintillators behind the telescopes and a single scintillator downstream centered around 0°. With all detectors in place, the total active solid angle subtended by this augmented Plastic Box was $\simeq 92\%$ of the full 4π. (This includes a 5% loss in solid angle due to shadowing by the target holder.)

The detection of a projectilelike fragment in either one of the solid-state telescopes provided the trigger for the Plastic Box. For each event, the pulse heights and timing signals of all silicon detectors and scintillators were recorded. This was accomplished via a CAMAC interface to the MODCOMP-based data-acquisition system.

Although the six walls allow for the registration of up to six hits, the accurate measurement of charged-particle multiplicity is hindered by the inability of the individual walls to discriminate between single and multiple hits. However, this was not judged to be a serious liability since the typical multiplicities were shown to be low in an earlier streamer-chamber study[15] of a similar reaction, 16.4-MeV/nucleon ^{16}O+CsI. The 250-MeV ^{16}O+^{nat}Sn reaction has been studied with the Plastic Box [Sn has nearly the same (Z,A) as CsI] and the deduced breakup probabilities[14] were found to be in agreement with the streamer-chamber results, indicating that the Plastic Box has $\simeq 4\pi$ efficiency for detecting light charged particles.

The experimental technique was motivated by the desire to distinguish those ejectiles arising from complete charge transfer from those leading to a third light charged particle. A third fragment can be liberated in one of three ways: sequential decay of the targetlike nucleus, sequential decay of the projectilelike nucleus, or a direct process associated with the collision itself. Of these, the first is a mechanism that does not change the identity, energy, or angular distribution of the primary ejectile. Thus, in order to suppress charged-particle emission, it is desirable to use a heavy target. Those particles emitted in spite of the large Coulomb barrier will have an almost isotropic distribution in the laboratory frame. It is the ability of the Plastic Box to provide rough position information via its segmentation that enables us to estimate and correct for this sequential target decay. Of the two remaining contributions to light charged-particle production, other studies[10,15-21] in this energy regime (10–20 MeV/nucleon) indicate that direct emission is less important than sequential decay.

All events with an ejectile trigger are characterized by the number, S, of scintillator walls that fired. Insofar as multiple hits on a single wall are ignored, S is a measure of the number of light charged particles emitted in coincidence with the observed ejectile. The $S=0$ yield corresponds to a complete transfer of charge in which the primary fragments are in charged-particle-bound states or else decay through fission or neutron emission. This process is referred to, operationally, as a transfer reaction. The $S \geq 1$ yields are referred to as breakup reactions. The correction for sequential target decay results in an increase in the $S=0$ yield compared to the raw value. The

remaining $S \geq 1$ yield will be assigned predominantly to sequential ejectile decay.

While the use of double walls of scintillator could, in principle, provide some particle identification, in practice the Plastic Box yielded little information on the identity of the charged fragment. This was due to two effects: the very high energy threshold for particle identification caused by the thickness of the inner wall, and the strong pulse-height dependence upon position. Therefore, it was not possible to reconstruct, on an event-by-event basis, the identity of a primary fragment that had decayed sequentially. This limitation has prompted the construction of a next generation of scintillator detector[22] having much better particle identification. In the present work, we rely on approximate, average reconstructions based upon known decay thresholds. These results are presented in a later section.

III. EXPERIMENTAL RESULTS

A. Results at 341 MeV

1. Cross sections

In Fig. 3, we show the relative yields for values of $S=0,1,\geq 2$ for ejectiles detected at 16°, plotted as a function of ejectile charge. The raw $S=0$ yield corresponds approximately to transfer reactions. The $S \geq 1$ yields represent breakup reactions but, in fact, as discussed in Sec. II, may contain contributions from sequential target decay via charged-particle emission. To correct for this
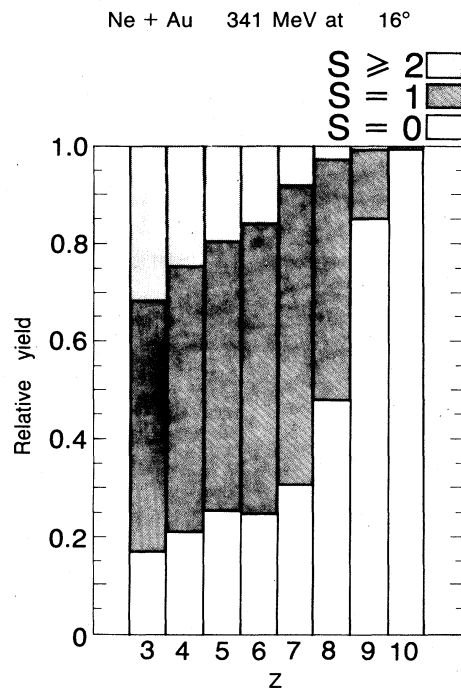

FIG. 3. The wall multiplicity, S, is plotted as a function of the charge of the trigger ejectile detected at 16°. The data are corrected for neutral events, but not for contributions from sequential target emission of charged particles.

target contribution to the value of S we exploit the angular information provided by the Plastic Box, as discussed below.

In Fig. 4, we show the distribution of charged particles in the six walls—a crude angular distribution—in coincidence with ejectiles at 16°. For all ejectiles, the coincident yield is concentrated in the forward walls (1 and 2). The backward walls (3 and 4) and the top and bottom walls (5 and 6) are essentially inaccessible to charged particles coming from projectile breakup. Therefore, the yield in these walls is assumed to come entirely from emission by the targetlike recoil. With the assumption that the emission is symmetric about 90° in the laboratory system, it is possible to calculate the contribution to walls 1 and 2 from the sequential decay of the target, and to define another class of events corresponding to complete charge transfer which is independent of the decay mode of the targetlike fragment. This is illustrated in Fig. 5, where the magnitude of this target correction can be seen. Given our assumptions, this correction is an upper limit. In all subsequent discussions, the $S=0$ yield will represent this corrected quantity. Figure 5 shows that the magnitude of the correction for target decay increases as the target captures larger amounts of charge. This is as expected since the excitation energy of the targetlike nucleus should be roughly proportional to the number of captured nucleons.

The charged-particle multiplicities associated with statistical decay of the targetlike fragments are listed in Table I. Only events in which no forward walls fired were considered, thus removing breakup contributions. In the table, we list the primary fragments [projectilelike (PLF)

FIG. 5. The relative yield of $S=0$ ejectiles is plotted as a function of ejectile charge, at the indicated angles. Results are shown with and without corrections for sequential charged-particle emission from the targetlike fragments.
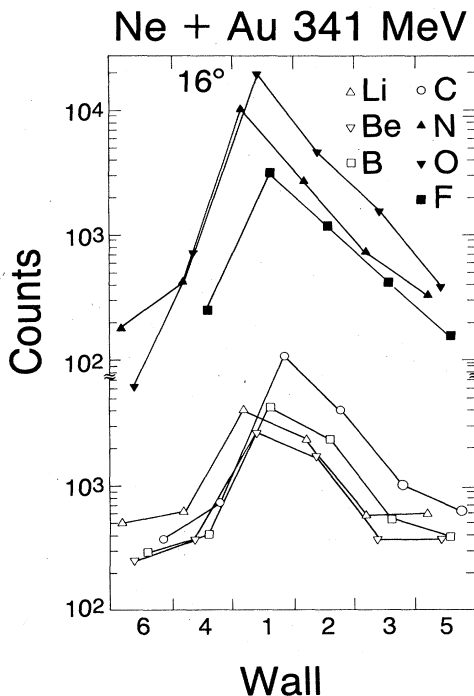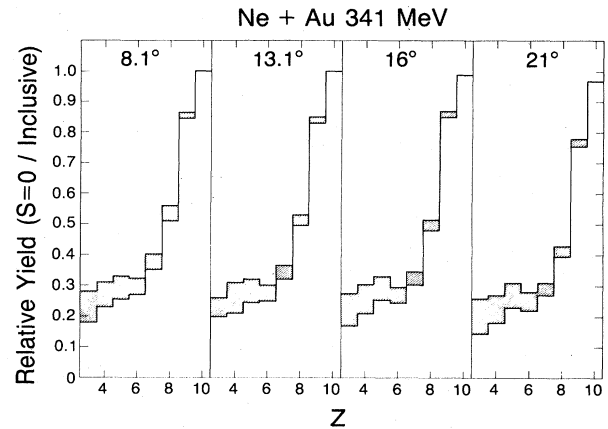

FIG. 4. The distributions of charged particles in the walls of the Plastic Box are shown for various coincident ejectiles. The numbering convention is the same as that of Fig. 1.

and targetlike (TLF)] as well as the average total excitation energies deduced from average ejectile energies. Also listed are the charged-particle multiplicities deduced from our analyses of the backward walls. As already seen in Fig. 5, target-recoil decay becomes more important for larger mass transfers (and higher excitation energies).

Statistical model calculations have been performed[23,24] to estimate the amount of charged-particle emission from targetlike fragments. The results were found to be consistent with our deduced contributions from sequential target decay. For example, the decay of the ^{203}Pb* nucleus (formed by ^{6}Li capture) was evaluated for an excitation of 101 MeV and a spin of $33\hbar$. These quantities correspond to a peripheral reaction with most of the excitation residing in the target. The calculated charged-particle multiplicity of 0.10 (0.08 and 0.02 for protons and alphas, respectively) agrees well with the experimentally deduced multiplicity of 0.09 for nitrogen ejectiles. This agreement indicates that contributions of sequential target decay to the Plastic-Box data are accurately identified.

The data of Fig. 5 indicate that the fluorine yield is dominated by $S=0$ events, but the relative importance of breakup increases rapidly as the ejectile charge further decreases by one and two units. Perhaps the most striking feature of Fig. 5 is the leveling off, or near constancy, of the $S=0$/inclusive ratio observed towards smaller values of Z. The transfer-to-inclusive ratios for ejectiles with $Z \leq 7$ are all roughly equal, and appear to have "relaxed" at a value of $\simeq 30\%$. This behavior is seen at all four measured ejectile angles. In fact, for each of the individual ejectiles the $S=0$/inclusive ratios are roughly constant over the measured angular range of 8°–21°.

In Fig. 6, the $S=0$ and inclusive (i.e., $S \geq 0$) double-differential cross sections, $d\sigma/d\Omega\,dZ$, are presented as a function of ejectile charge and scattering angle. The classical grazing angle for this reaction is $\simeq 17°$. For both the $S=0$ and the inclusive yields, the cross sections appear to be peaked forward of this value, an effect becoming more pronounced for the lighter ejectiles.

In order to determine ejectile production cross sections,

TABLE I. Estimated contributions from sequential charged-particle decay of targetlike fragments. For each binary channel (PLF and TLF), the average ejectile energy and estimated total excitation energy is indicated, along with the deduced multiplicity of charged particles.

		341-MeV ^{20}Ne$+^{197}$Au $\theta=16°$		
PLF	TLF	E_{PLF} (MeV)	E^*_{tot}(approx) (MeV)	$M_{p,\alpha}$ (exp)
Li	Rn	84	220	0.32
Be	At	110	200	0.28
B	Po	134	160	0.19
C	Bi	170	140	0.13
N	Pb	211	110	0.09
O	Tl	256	70	0.07
F	Hg	293	10	0.03

we have performed inclusive measurements of differential cross sections over a much wider range of ejectile angle than could be accommodated in the coincidence work. The results are presented in Fig. 7. The angle-integrated inclusive cross sections at 341 MeV, obtained from these differential cross sections, are plotted in Fig. 8 along with values obtained at several other beam energies by the Hahn-Meitner group.[25] Both sets of results exhibit the same systematic trends and appear to be consistent with each other.

Total angle-integrated yields for transfer reactions were obtained by integrating the inclusive angular distributions weighted by the $S=0$/inclusive ratio for each ejectile. Since the $S=0$/inclusive ratios were found to change slowly over the angular range 8°–21°, we have extrapolated this ratio to angles lying outside of this range. (This prescription is illustrated in Fig. 9 for oxygen, carbon, and lithium ejectiles.) The error incurred in using such an extrapolation is small: for angles smaller than 8°, contributions to $d\sigma/d\theta$ are diminished by the $\sin\theta$ factor; for angles greater than 21°, the inclusive yields drop rapidly, and the contribution from this angular region to both inclusive and $S=0$ yields is small. Figure 10 shows the absolute cross sections for the $S=0$, $S\geq1$, and inclusive reactions at 341 MeV. The uncertainty in the absolute values is

$\simeq\pm20\%$. The relative errors are $\simeq\pm10\%$.

These uncertainties are due, in part, to uncertainties in the efficiency of the Plastic Box to detect all charged particles; e.g., there are regions that are shadowed by the target holder and solid-state telescopes. In the case of the target holder, this shadowing is $\simeq5\%$ of 4π. However, only target-emitted particles are likely to be blocked, and in equal amounts forward and backward. Therefore, the target correction to the coincident data will not be affected. Analysis of the events in the downstream detector at 0° indicates that relatively few light particles from breakup are lost along the beam axis. Of more concern is the shadowing by the telescopes, since the projectile-related particles are focused in the direction of the ejectile. The magnitude of this effect has been estimated by assuming that the telescopes obscure a portion of the breakup cones of decaying ejectiles, and has been found to be no bigger than $\simeq6\%$. (The cross sections shown do not have this dead-space correction.)

Since the Plastic Box detects only charged particles, it is important to know whether the sequential decay of an ejectile will result in the emission of a neutron instead of a proton or alpha. A study of the decay thresholds associ-
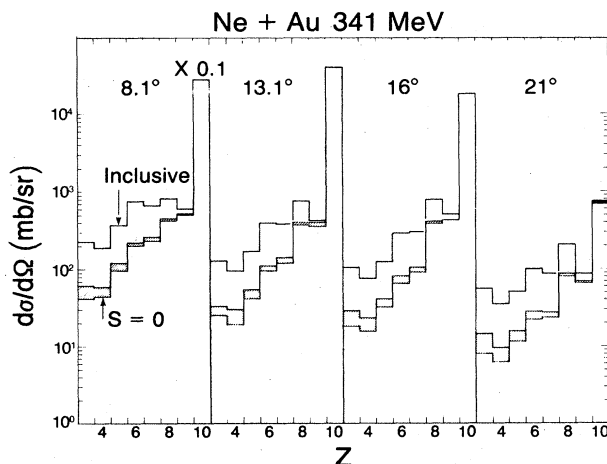

FIG. 6. The differential cross sections versus ejectile charge are plotted for various angles. The yields shown represent inclusive and $S=0$ cross sections. The shaded areas represent the correction for target decay.
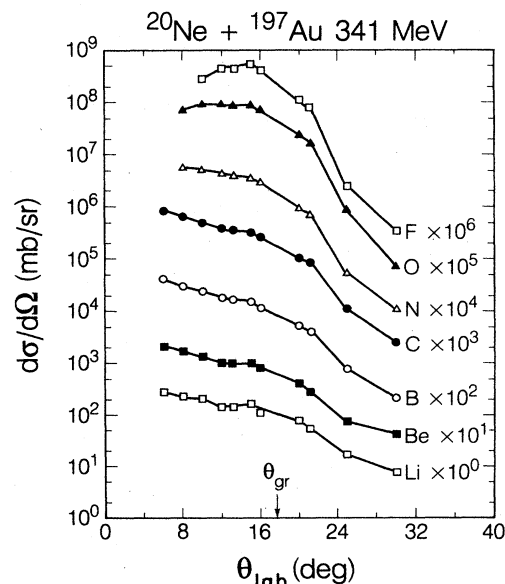

FIG. 7. Particle-inclusive angular distributions are plotted for various ejectiles.
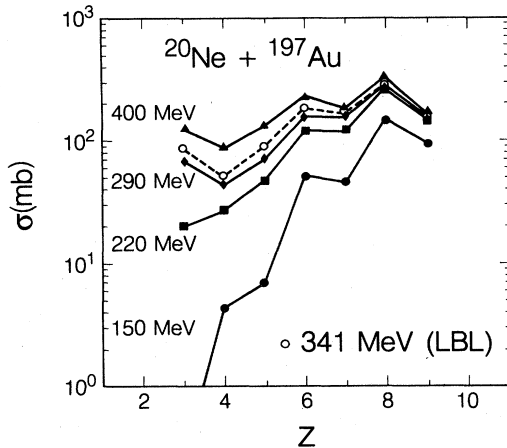
FIG. 8. The angle-integrated inclusive yields at 341 MeV are plotted as a function of ejectile charge. Also plotted are inclusive cross sections measured at several other bombarding energies by the HMI group (Ref. 25).

ated with the most abundant isotopes observed in this work indicates that ^{10}Be, ^{13,14}C, and ^{17}O will preferentially decay via the emission of a neutron. (In the case of ^{9}Be, alpha particles are emitted following neutron decay to ^{8}Be.) Therefore, the $S = 0$ beryllium and carbon cross sections (and, to a lesser extent, the $S = 0$ oxygen) will be "contaminated" by neutron breakup. However, the presence of neutron decay does not affect the interpretation of the $S = 0$ and $S = 1$ yields in terms of charge-transfer and charge-breakup probabilities.

2. Energy spectra

The particle-inclusive energy spectra of ejectiles from lithium to fluorine are shown in Fig. 11. As can be seen,

FIG. 10. Inclusive cross sections are plotted as a function of ejectile charge. Also shown are the deduced transfer and breakup components.
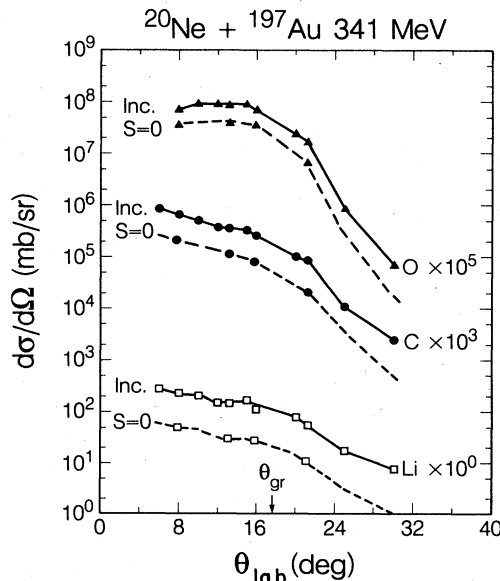

FIG. 9. The decomposition of the inclusive angular distributions into transfer yields is illustrated for three ejectiles. The $S = 0$ data points are derived from the Plastic-Box work.
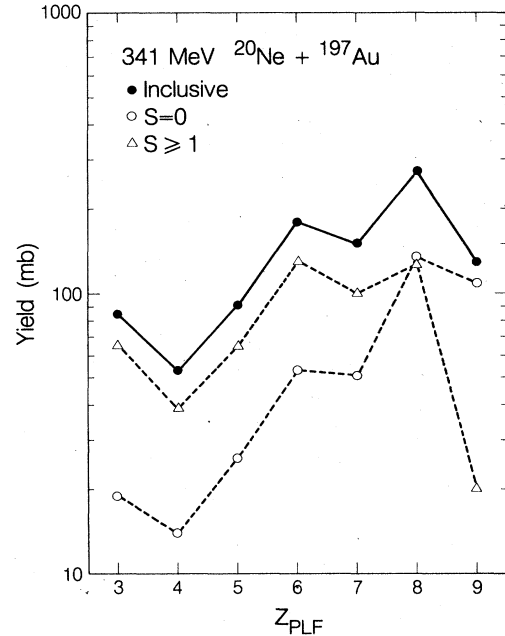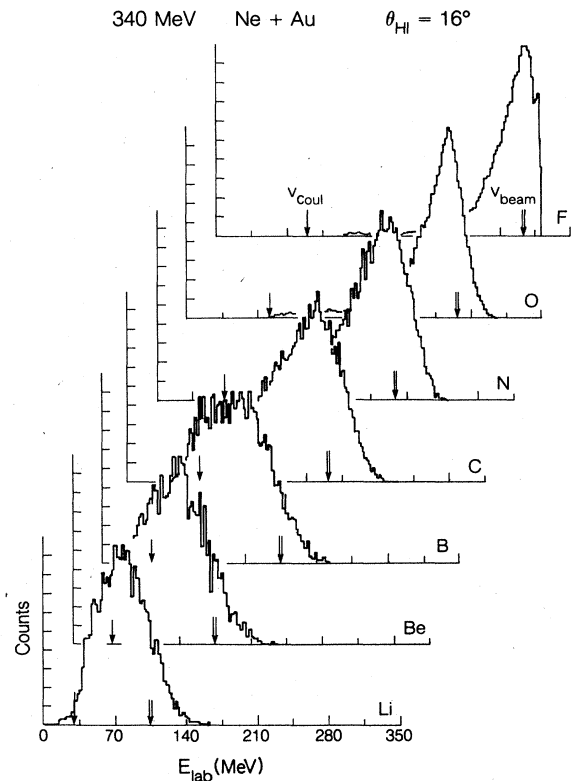

FIG. 11. Particle-inclusive energy spectra are shown for various ejectiles. The arrows indicate ejectile energies corresponding to beam-velocity fragments as well as those emitted with the Coulomb energy.

the peak energies of all ejectiles are correlated approximately with the beam velocity. In addition, for the heavier ejectiles, the distribution does not extend down to the respective ejectile Coulomb barriers. These observations suggest that the reaction mechanism producing the heavier observed ejectiles is of a quasielastic nature. Although there is increasing inelasticity for the lighter ejectiles, it will be shown in Sec. V that the peak energies can be reproduced by calculations assuming a quasielastic process.

As was done with the ejectile cross sections, the energy spectra can be decomposed into those arising from transfer and those from breakup. This is illustrated in Fig. 12, where the two components of the spectra are shown for ^{16}O and ^{17}O fragments detected at 16°. In order to make a quantitative, unambiguous, and global comparison of many different spectra, the first four central moments of each energy distribution were extracted. These moments—mean $\bar{E}$, width σ, skewness γ_1, and kurtosis β_2—are defined by the relations:

$$\bar{E} = \langle E \rangle ,$$

$$\sigma^2 = \langle (E - \bar{E})^2 \rangle ,$$

$$\gamma_1 = \langle (E - \bar{E})^3 \rangle / \sigma^3 ,$$

and

$$\beta_2 = \langle (E - \bar{E})^4 \rangle / \sigma^4 .$$

The results are shown in Fig. 13 for the most abundant isotopes, observed at 16°.

What is remarkable about these moments is the general similarity of the $S = 0$ and $S = 1$ components for each isotope. Only for the heaviest ejectiles ($Z = 8,9$) are there any significant differences between the moments associated with transfer and those with breakup. The means, in particular, track very well, with the only obvious differences occurring for $Z \geq 8$.

B. Results at 220 MeV

In order to study the relative importance of the transfer and breakup mechanisms at a lower energy, the experiment conducted at 341 MeV was also performed at 220 MeV (11 MeV/nucleon). This represents a 35% decrease in bombarding energy, with the corresponding reduction in relative kinetic energy above barrier being roughly a factor of 2.

Data were collected for those events triggered by ejectiles detected at 15° and 20°. The number of charged particles versus wall number is shown in Fig. 14. For ejectiles close to neon, the shapes of the wall distributions resemble those at the higher bombarding energy. However, for $Z \leq 6$, there are relatively fewer charged particles in the back walls. This is reasonable since at 220 MeV multinucleon transfer (via a fast, quasielastic process) imparts less excitation energy to the ^{197}Au target than at 341 MeV. This leads, in turn, to a smaller cross section for charged-particle evaporation.

In order to assess the breakup probability, we must again subtract the effect of sequential target emission. This leads to the results shown in Figs. 15 and 16 where, as at 341 MeV, the $S = 0$/inclusive ratios and the double-differential $S = 0$ and inclusive yields are plotted versus ejectile charge.
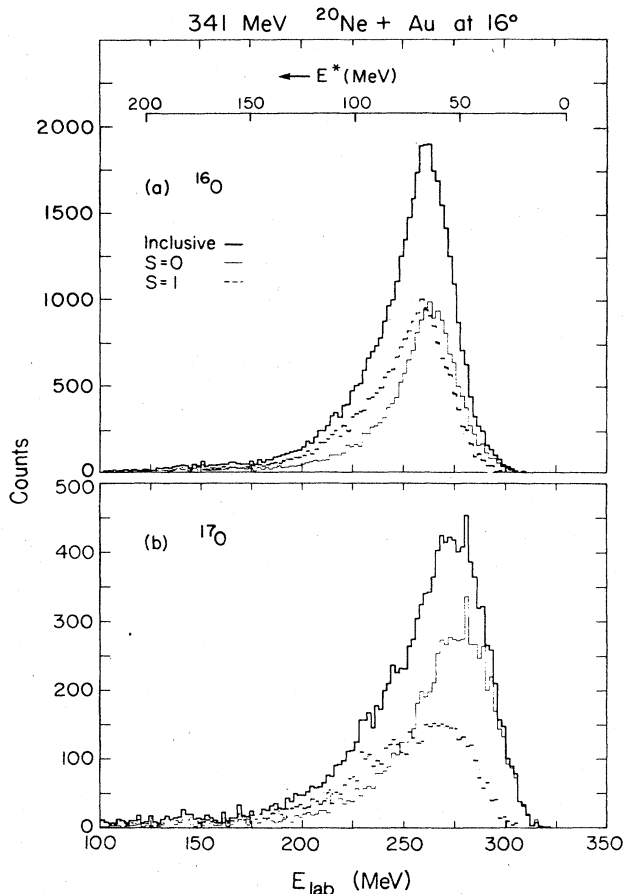

FIG. 12. The decomposition of particle-inclusive energy spectra is illustrated for two specific ejectiles. Inclusive spectra are shown, as well as transfer and breakup spectra.
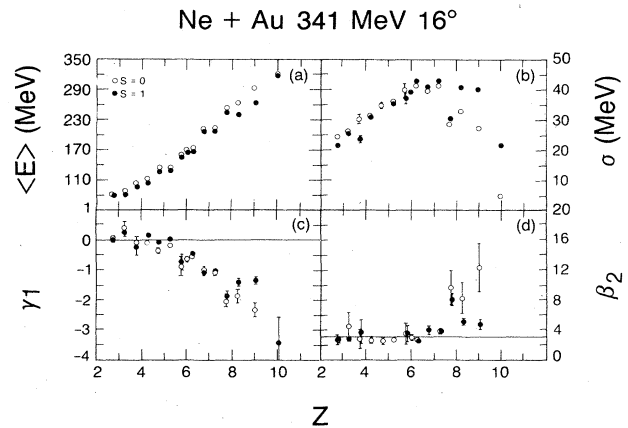

FIG. 13. The central moments of the ejectile energy spectra, measured at 16° in the laboratory: (a) mean, (b) width, (c) skewness, (d) kurtosis. The moments are shown for transfer and breakup yields of (left to right) $^{6,7}Li$, $^{7,9}Be$, $^{10,11}B$, $^{11,12,13}C$, $^{14,15}N$, $^{16,17}O$, ^{19}F, and ^{20}Ne. Elastic scattering has been excluded from the ^{20}Ne spectrum.
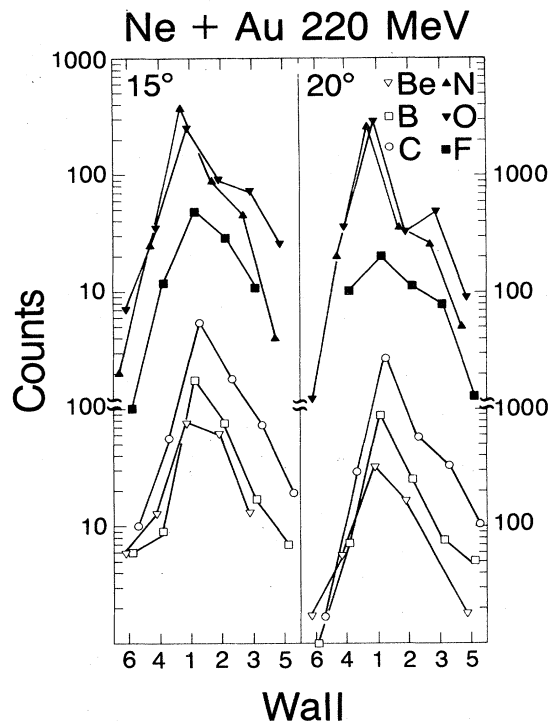
Ne + Au 220 MeV

FIG. 14. The distributions of charged particles in the walls of the Plastic Box are shown for various coincident ejectiles. The numbering convention is the same as that of Fig. 1.

The transfer/inclusive ratios at 220 MeV exhibit a behavior that is qualitatively similar to that observed at 341 MeV. Specifically, the $S=0$ component dominates the fluorine yield, with the $S=0$/inclusive ratio dropping rapidly with decreasing ejectile charge. This drop appears
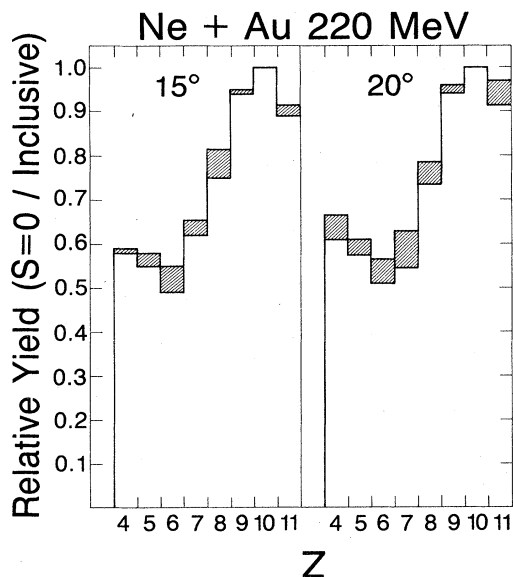
Ne + Au 220 MeV

FIG. 15. The relative yield of $S=0$ ejectiles is plotted as a function of ejectile charge, and at the indicated angles. Results are shown with and without corrections for sequential charged-particle emission from the targetlike fragments.
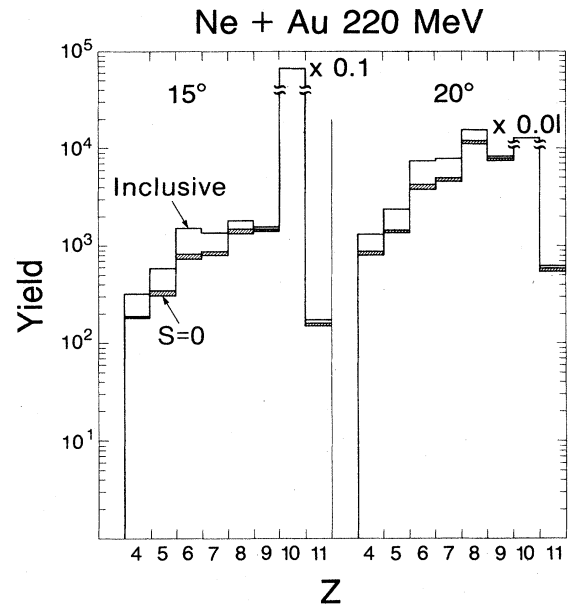
Ne + Au 220 MeV

FIG. 16. The differential cross sections versus ejectile charge plotted for various angles. The yields shown represent inclusive and $S=0$ cross sections. The shaded areas represent the correction for target decay.

to level off by $Z=7$, and reaches values of $\simeq 60\%$ and $\simeq 30\%$ at 220 and 341 MeV, respectively. Therefore, the main difference in the results obtained at the two bombarding energies is the $S=0$/inclusive ratio for the massive charge-transfer processes.

Due to the unavailability of data for angles beyond 21°, we do not know the $S=0$/inclusive ratio near the grazing angle at 220 MeV. However, it has already been shown that the $S=0$/inclusive ratios at 341 MeV are rather insensitive to scattering angle over a large angular range. Assuming that this is the case at 220 MeV as well, one can use the measured ratios at angles well forward of grazing to scale the total inclusive yield. We have taken inclusive cross sections measured at 220 MeV by the HMI group[25] and have applied our experimental $S=0$/inclusive ratios to determine, element by element, the transfer and breakup contributions. This is shown in Fig. 17 where, as at 341 MeV, the inclusive ejectile cross sections are decomposed into $S=0$ and $S=1$ yields.

IV. PRIMARY EJECTILE YIELDS

A. Reconstruction of primary cross sections

It would be very instructive to compare the transfer and breakup cross sections derived in the previous section with predictions of reaction models. However, while there exist models that make predictions of the primary ejectile yields, extensions of these models to include the effects of sequential decay are difficult to make. For this reason, comparisons with inclusive measurements usually make the ansatz that the observed secondary yields represent the primary ones. Such an assumption is clearly a tenuous one at the bombarding energies being considered in the present work since we observe large breakup cross sec-
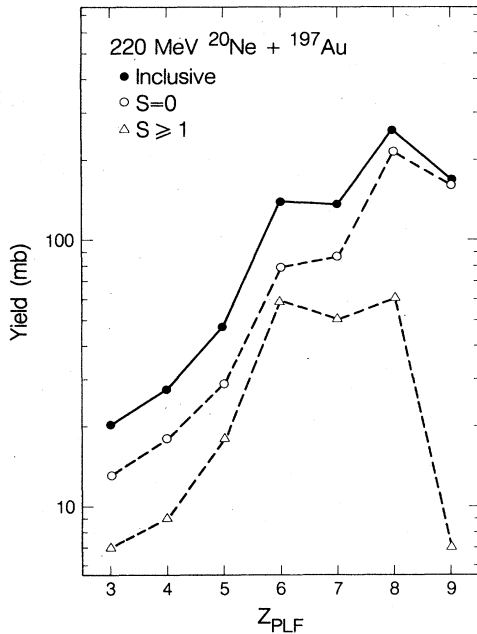
FIG. 17. Inclusive cross sections are plotted as a function of ejectile charge. Also shown are the deduced transfer and breakup components.

FIG. 19. The reconstruction of primary ejectile yields is illustrated schematically for the 341-MeV data.

tions. Therefore, we have constructed the primary ejectile distributions from the experimental data, using the following approximations.

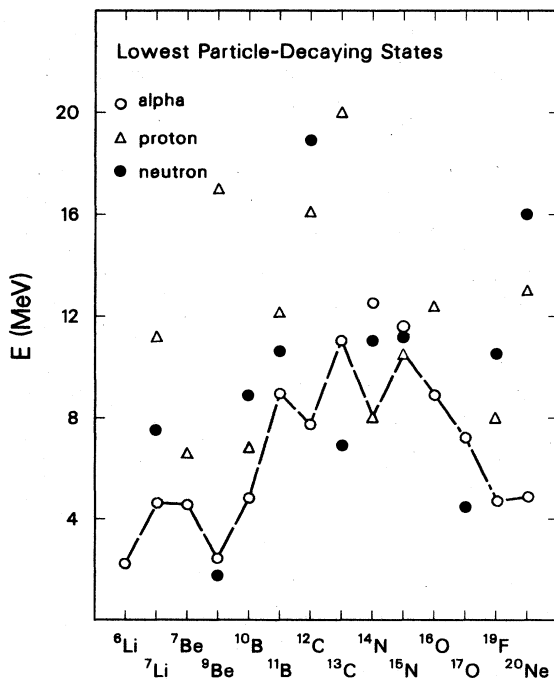We assume that the $S \geq 1$ yields arise from the sequential proton or alpha decay of an excited primary projectilelike fragment. (This assumption is borne out by other studies[10,15−21] of heavy-ion breakup in this energy regime which suggest that prompt emission, if it exists, is much less important than the sequential breakup channel.) This presents two possible decay paths leading to each observed ejectile. We make the further assumption that the decay mode of each primary fragment will be dominated by its lowest threshold. In almost all cases, the alpha threshold of a primary fragment is lower than the proton threshold. (The energies of the first alpha-, proton-, and neutron-decaying states of the most prominent ejectiles are indicated in Fig. 18). Therefore, in most cases, the $S = 1$ events will be fed via alpha-decaying states. (This assumption is supported by more recent coincidence experiments,[26]

FIG. 18. The energy of the lowest alpha-, proton-, and neutron-decaying states are shown for the most prominent ejectiles.

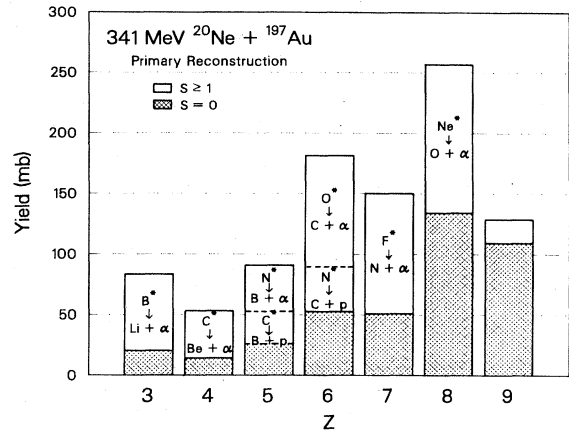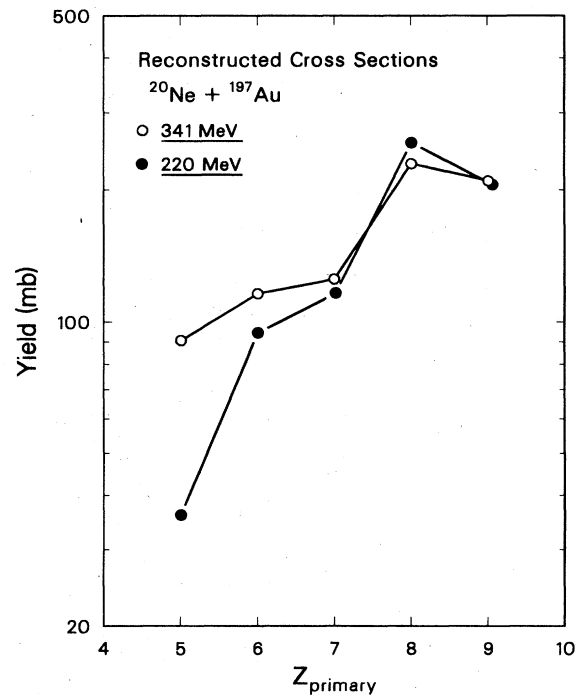FIG. 20. The reconstructed primary cross sections are plotted versus primary ejectile charge, as deduced from data at both bombarding energies.

which indicate a preponderance of alpha particles accompanying breakup.)

The low proton threshold of nitrogen provides an exception to this rule. As a result, the $S = 1$ carbon cross section could be expected to contain contributions from both oxygen and nitrogen breakup. Similarly, the $S = 1$ boron yield should be nonexistent (insofar as our ansatz, that only the lowest thresholds contribute, is valid). For these two cases, we have assumed that both proton and alpha sequential decays contribute to the observed breakup yield, and further assume that the relative contributions scale with the experimental $S = 0$ yields of the two possible primary nuclei. This provides us with a reconstruction of primary yields as outlined schematically in Fig. 19.

The presence of low-lying neutron-decaying states among some of the ejectiles has already been noted. While this must be considered in evaluating the deduced breakup probabilities, this does not affect the accuracy of the reconstruction since the primary yields are summed over isotope.

The reconstruction procedure just outlined generates primary cross sections over the range of primary charge $Z = 5$—9. It should be noted that the breakup of lithium and beryllium would result in $S = 1$ alpha and proton events. However, such events could also come from the breakup of heavier ejectiles, in which the alpha or proton is detected in a telescope and the projectilelike fragment triggers the Plastic Box. Thus, the data do not allow us to estimate the primary lithium and beryllium yields. Also, the instability of ^8Be does not allow us to measure an $S = 1$ ^8Be cross section. Therefore, we miss a cross section that should have been added to the primary carbon yield in our reconstruction algorithm. For this reason, the reconstructed carbon yield will underestimate the abundance of primary carbon fragments.

The results of the experimental reconstruction of the primary ejectile charge yields are shown in Fig. 20, at both 11 and 17 MeV/nucleon. The cross sections for the production of the heaviest ejectiles are remarkably similar at both bombarding energies. The higher beam energy is seen to enhance the yields of light fragments arising from massive charge transfer. It is immediately obvious that the large cross sections observed for the production of light ejectiles at higher beam energies are due to two effects: increased excitation energy in the primary fragment as well as greater charge transfer prior to breakup.

B. Model predictions of yields

In Sec. III A, we noted that the 341-MeV angular distributions (Fig. 7) were, for most ejectiles, peaked forward of the classical grazing angle. This forward peaking was more pronounced for the larger mass transfer, i.e., for the lighter ejectiles. Such a phenomenon is consistent with a highly geometrical process, of the sort embodied in the overlap model of Harvey and Homeyer.[27] It is also consistent with angular-momentum limitations as employed in the sum-rule model of Wilczynski et al.[28] In both cases, the lighter ejectiles will arise from trajectories with smaller impact parameters; the increased importance of the nuclear force would then cause scattering to smaller

(or negative) angles.

The sum-rule model has previously been employed[6,28] in connection with studies of incomplete fusion and massive transfer. It assumes that the production of two primary fragments (binary exit channels) is governed by the same mechanism found in fusion. The projectilelike fragments are associated with entrance-channel partial waves that exceed some l_{cr} for fusion. The sum rule results in a competition among the various possible ejectiles (and fusion) for the available cross section. This competition is governed by limiting l waves (which represent an extension of the l_{cr} concept to all exit channels) as well as phase-space limitations. The latter are modeled by using probabilities derived from Q_{gg} systematics.

The sum-rule model has been applied to the 220- and 341-MeV $^{20}Ne + ^{197}Au$ reactions (Fig. 21). As was done in Ref. 28, the calculations included the inelastic and few-nucleon-pickup channels. For the purposes of comparison with experiment, all cross sections are summed over isotope. Also, the predicted ^8Be yield is excluded from the primary distributions since it is excluded in our experimental data. Calculations were performed in which all input parameters were varied. For the most part, the only substantial changes in cross section occurred for isotopes within a given elemental group. The total elemental yield, however, was relatively insensitive to variations in the Coulomb-radius (r_C) and l-wave-diffuseness (Δl) parameters. (The values used in the calculations are indicated in the caption to Fig. 21). More critical was the value of the phase-space parameter, T, since this "temperature" af-
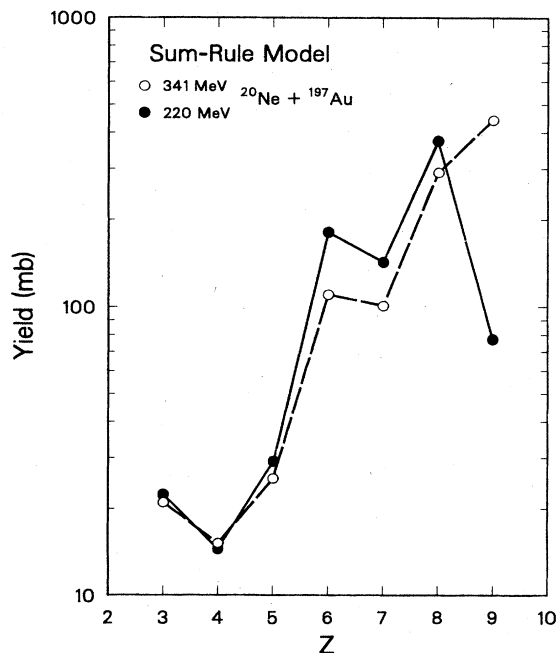

FIG. 21. Ejectile yields as predicted by the sum-rule model (Ref. 28) are shown at both bombarding energies. Calculations were performed using $r_C = 1.5$ fm, $\Delta l = 1.7\hbar$, and $T = 4$ and 5 MeV at 220- and 341-MeV bombarding energies, respectively. The ^8Be cross sections have been excluded.

fects the Q_{gg} systematics.

In the earlier incomplete-fusion work,[6,28] the sum-rule predictions were compared to the yields of only the binary channels. Therefore, the breakup channels were excluded from the experimental cross sections. In the present work, these binary reactions are represented by the $S = 0$ yields. For this reason, the phase-space parameter T was adjusted to reproduce the $S = 0$ cross sections of the lightest ejectiles. The results of the calculations are shown in Fig. 21, and are compared with the $S = 0$ yields in Fig. 22.

As can be seen in Fig. 21, the predicted yields of the lightest ejectiles (i.e., the most-massive transfer) are essentially independent of the bombarding energy. There is a sharp rise in cross section in going from boron to carbon, a reflection of the respective Q values. The large difference in the predicted fluorine yields are due to the additional partial waves brought into the reaction at 341 MeV, with these l waves preferentially enhancing few-nucleon transfer.

The agreement between the $S = 0$ yields and the sum-rule predictions for $Z = 3-5$, shown in Fig. 22, was achieved with reasonable choices of the phase-space parameter. However, the model consistently overpredicts the binary cross sections for the heavier ejectiles. This is particularly surprising in view of the fact that the experimental $S = 0$ yields should be further enhanced by quasi-elastic mechanisms not considered in the sum rule. However, the application of the sum rule to the binary channels, while an improvement over comparisons to the inclusive yields, is certainly not correct when the breakup
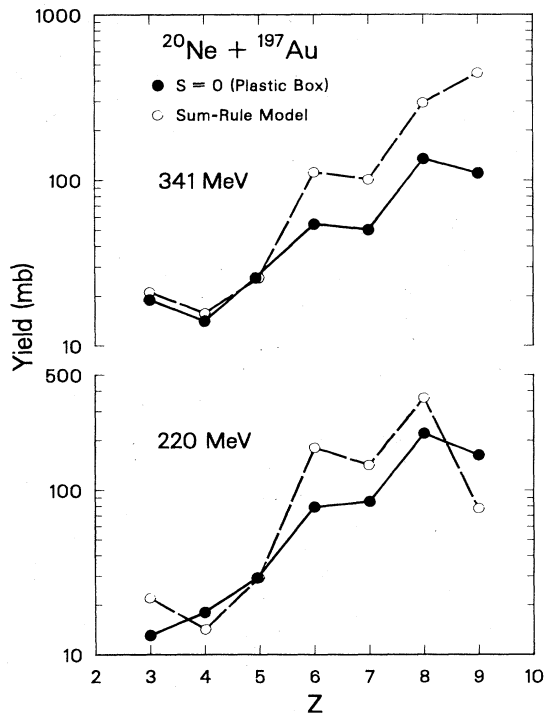

FIG. 22. The predictions of the sum-rule model are compared with the $S = 0$ cross sections at 220 and 341 MeV. The sum-rule parameters are given in the previous figure caption.

and $S = 0$ cross sections are comparable, as is the case in our work. Therefore, in Sec. IV C, comparisons will be made with the reconstructed primary yields. While it is true that the use of Q_{gg} systematics may be tenuous when ejectile excitations are large (as is the case for part of the primary yield), the cross sections must, by definition, obey a sum rule. This is a necessary condition not met with the $S = 0$ yields.

Whereas the sum-rule model views fragment production as an extension of the fusion process, subject to angular momentum limitations, the overlap model[27] considers a reaction mechanism that is more quasielastic in nature. The complete fusion cross section is either taken from experiment or from a separate model. Nucleon transfer for the impact parameters beyond the fusion limit is governed by the requirement that the transferred mass be contained in the spatial overlap between target and projectile.[29] Such a geometry has been used in abrasion-ablation models[30] of high-energy reactions.

The two requirements, (a) that the transferred nucleons will interact strongly enough with the target to be removed from the projectile, and (b) that the ejectile thus formed will escape without further interaction, together restrict the range of ejectile masses that are formed at given impact parameter. The two requirements are most easily satisfied when there is a high probability that the two parts of the projectile will be further apart than some critical distance. This probability is taken from the fragmentation model of Friedman,[31] where it is shown to be greatest when the separation energy of the two parts of the projectile is low and their N/Z ratios are close to that of the projectile.

The overlap model applies a "sum rule" over impact parameter rather than partial-wave space. Since fragment formation begins only beyond the energy-dependent fusion radius, the choice of r_{fusion} is critical. Variations in this radius will affect the predicted yields associated with the most central collisions, i.e., the most massive transfers. (This is in contrast to the sum-rule model, where the few-nucleon transfers were sensitive to the choice of l_{max}.)

A simple parametrization of the fusion cross section as a function of r_{fusion} was employed. The fusion radius was then adjusted to reproduce fusion cross sections derived from either experiment or fusion systematics. Similarly, a maximum radius of interaction, $r_0(A_1^{1/3} + A_2^{1/3})$, which affects the few-nucleon-transfer channels and the reaction cross section, was found to reproduce measured cross sections with r_0 equal to 1.4 fm. The Friedman probabilities were calculated using $b = 0.3$. This parameter was fit to the data, and was found to give somewhat better results than the value $b = 0.4$, which Friedman extracted[31] from ^{12}C- and ^{16}O-induced yields.

Just as the sum-rule model introduces a partial-wave diffusivity parameter, so the overlap model makes use of a width, Δ_R, to characterize the distribution of impact parameters giving rise to a particular ejectile mass. This width was adjusted to give the best fit to experimentally derived ejectile cross sections. The best value was found to be 0.65 fm, corresponding to rather strong localization.

The primary fragment yields predicted by the overlap model are shown in Fig. 23 for both 220 and 341 MeV.
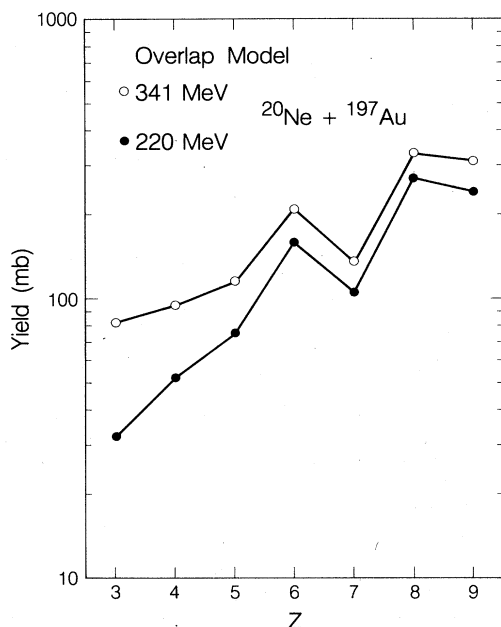
FIG. 23. Primary yields as predicted by the overlap model (Ref. 27) are shown at both bombarding energies. Calculations were performed using $r_0 = 1.4$ fm, $\Delta_R = 0.65$ fm, and $b = 0.3$. The ^{8}Be cross section has been excluded.

As was done for the sum-rule model, all cross sections are summed over isotope and the ^{8}Be yield is explicitly excluded. At both energies, the elemental distributions exhibit a much flatter Z dependence than those from the sum-rule model. Also, unlike the sum-rule model, it is the large charge transfer that is most sensitive to bombarding energy.

In the next section, comparisons will be made between the reconstructed cross sections and those from the models already cited.

C. Comparison of reconstructed and predicted yields

In Figs. 24 and 25, the sum-rule and overlap model predictions at 220 and 341 MeV are plotted, along with our reconstructed primary yields.

At 220-MeV bombarding energy (Fig. 24), both models enjoy success in generating the primary $Z = 6-8$ yields. The drop in the sum-rule-predicted fluorine cross section is due to the truncation of the l-wave summation, and therefore represents a detail of the calculation rather than physics. Also, while both models overpredict the carbon yield, it has already been noted that the primary reconstruction underestimates carbon due to the absence of ^{8}Be in our data. However, the primary boron yield (and consequently, the large drop from carbon to boron) is reproduced only by the sum-rule model, with the overlap model exhibiting a more gradual fall.

At 341 MeV (Fig. 25), the models are again in qualitative agreement for the heaviest ejectiles. The primary carbon yield, allowing for the underestimate of the reconstruction, is somewhere in between the two predictions. However, the boron cross section is again reproduced by just one of the models, this time the overlap model. It
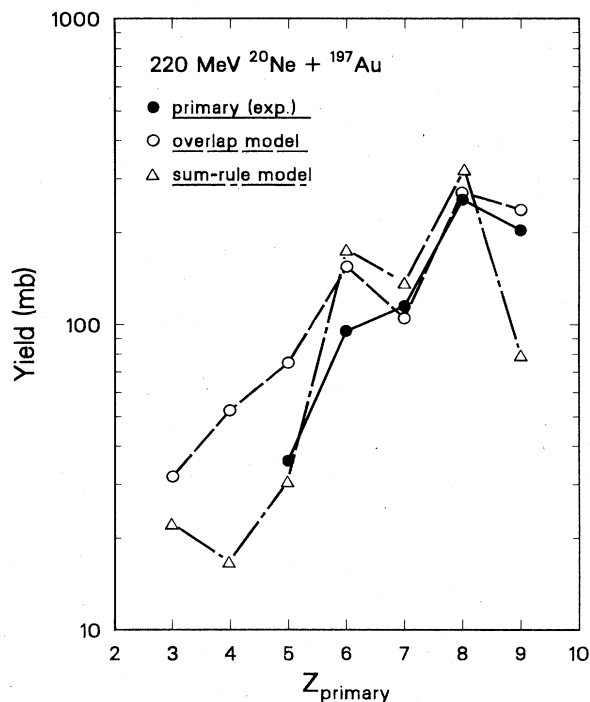

FIG. 24. The predictions of the sum-rule and overlap models at 220 MeV are compared with the reconstructed primary cross sections.

should be recalled that the sum-rule calculations were originally fitted to the $S = 0$ yields. Therefore, in principle, it would be possible to improve the agreement between the sum-rule and primary data at 341 MeV, espe-
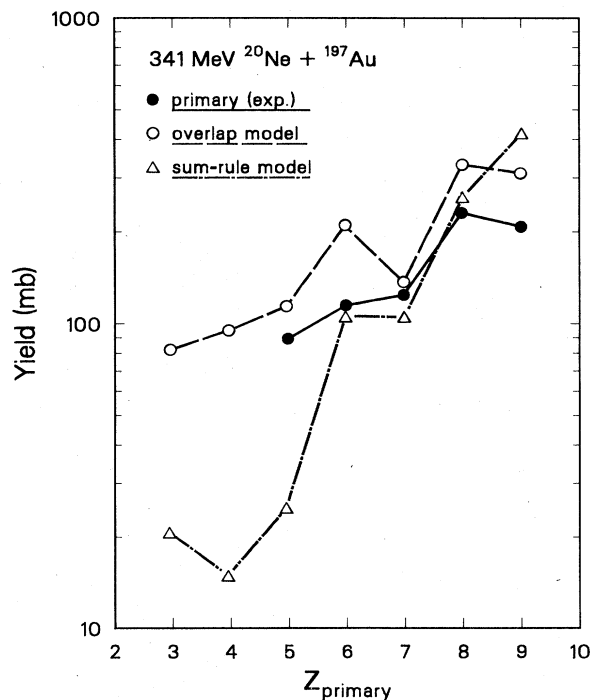

FIG. 25. The predictions of the sum-rule and overlap models at 341 MeV are compared with the reconstructed primary cross sections.

cially the boron cross sections. However, to do so would require using an extremely large value of the phase-space parameter ($T \simeq 15$ MeV). This, in turn, leads to fusion cross sections of the order of 50 mb, and so must be rejected as unphysical.

For the system considered in the present investigation, both the sum-rule and overlap models do a fairly good job of predicting the reconstructed primary yields. The channel corresponding to the largest charge transfer (boron) is best reproduced by the sum-rule model at 11 MeV/nucleon and by the overlap model at 17 MeV/nucleon. This is consistent with the physics inherent in each model. At the higher beam energy, the large ejectile excitations make it more difficult to scale the phase space with the Q_{gg} in a simple manner. Conversely, at lower energies, the simple geometric picture of the overlap model should start to fail. However, in addition to absolute cross sections, each model predicts the transferred angular momentum. Comparison of experimental[32] and theoretical calculations for this latter quantity should be part of a complete evaluation.

D. Survival fraction of the primary ejectiles, and the division of excitation energy

From the reconstructed primary yields, we can calculate the probability that an ejectile will "survive" the transfer process without undergoing sequential charged-particle decay. This is just the ratio of its $S = 0$ cross section to its primary cross section, and is of greater physical significance than the $S = 0$/inclusive ratio. These survival fractions, calculated at 341 and 220 MeV, are shown in Fig. 26. The smaller survival fractions at the higher
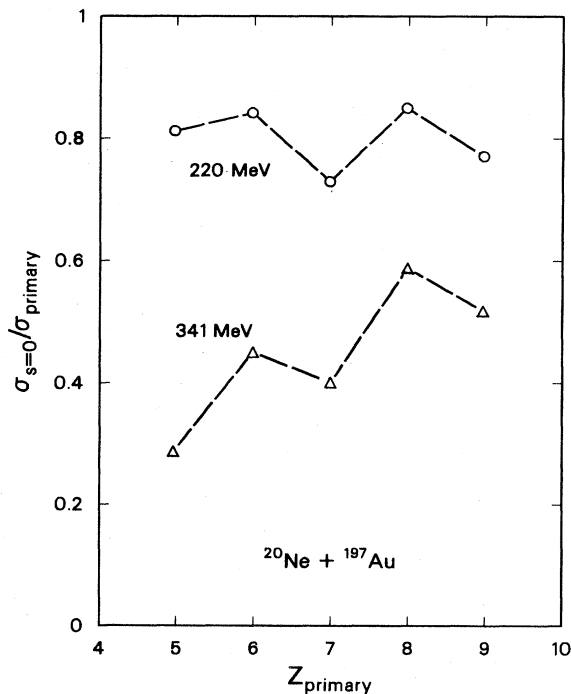
bombarding energy can be understood in terms of the greater excitation associated with nucleon transfer at high energies. There is also an apparent odd-even effect, suggesting that even-Z fragments have enhanced survival fractions. Alternatively, this may be caused by the presence of sequential neutron decay, which depletes the $S = 1$ cross sections. Since the carbon and oxygen yields are most affected by this contamination of the $S = 0$ probabilities, the shift will be largest for them. Also, since the primary carbon yield is underestimated by the reconstruction, the survival fraction will be overestimated.

However, the striking aspect is that the survival fractions associated with the massive charge-transfer channels are as large as they are, given that the massive-transfer events are characterized by very large total excitation energies. This indicates that most of the excitation energy resides with the targetlike fragment. If, for example, we assume that the excitation energy is divided according to the ratio of the primary masses (as would be the case for equal temperatures), then the values of $S = 0$/primary ratios can be reproduced qualitatively. This is illustrated in Fig. 27, where the first particle-decaying states of the various ejectiles are compared with the average excitation energies deposited in the primary ejectiles assuming the above division. As can be seen, the mass-asymmetric division of excitation results in ejectile excitation energies that track roughly with the decay thresholds. (A quantitative estimate of the survival fraction would require knowledge about the width of the excitation-energy distribution in the light primary fragment.) On the other hand, an equal division of excitation energy (solid lines in Fig. 27) leads to results that are clearly inconsistent with the

FIG. 26. The survival fractions are plotted as a function of primary ejectile charge at both bombarding energies.
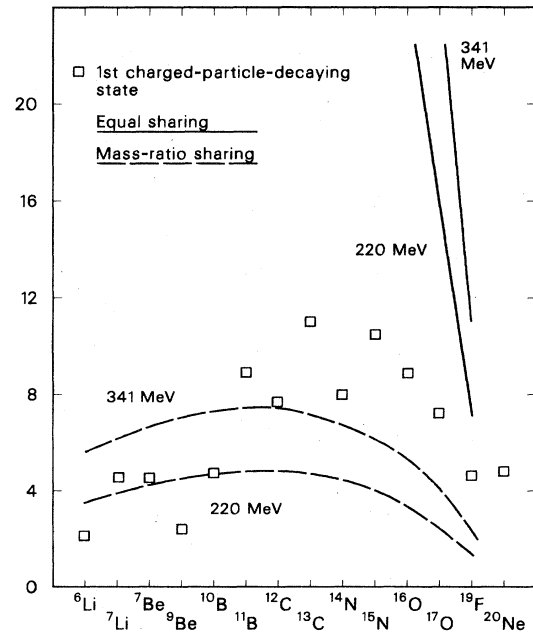

FIG. 27. The mean excitation energies of the primary fragments are calculated assuming either equal sharing of excitation or division according to the exit-channel mass ratio. Also shown are the energies of the first charged-particle-decaying states of the most prominent ejectiles.

experimental yield of bound ejectiles.

Recently, there have been other experimental studies that have focused on the question of excitation-energy division. Awes et al.[33] have studied ejectiles from 15.3-MeV ^{58}Ni+^{197}Au reactions, while Vandenbosch et al.[34] have examined 8.5-MeV/nucleon ^{56}Fe+^{238}U. In both cases, the results for the smaller total energy losses were much closer to the equal-excitation limit. An equal-excitation fractionation is predicted by nucleon-exchange models, provided that the mass-fluxes in each direction are the same and that the interaction time is too short to permit subsequent equilibration. The much more asymmetric division observed, in the present work, for projectilelike fragments lighter than neon may be explained in terms of a unidirectional mass flow from projectile to target. In this case, the target, which captures high-velocity nucleons from the projectile, absorbs most of the excitation energy. This is, of course, what happens in direct stripping reactions. Such an asymmetric division thus does not require the assumption of energy equilibration and equal temperatures.

Detailed experimental studies are currently under way to learn more about the division of excitation energy in the primary fragments by measuring the charge, energy, and angle of the emitted light particles.

V. COMPARISONS
OF ENERGY SPECTRA WITH MODELS

The overall similarity between the transfer and breakup components of the spectra for a given ejectile has already been noted. Unfortunately, neither of the two models discussed in Sec. IV is able to make predictions concerning the distribution of ejectile energies. Both models assume a dissociation of the projectile, so that the most probable ejectile energies correspond to the beam velocity.

Predictions of the most probable velocity of the primary ejectile[29] can be made with Brink's semiclassical theory[35] for transfer reactions. This model requires that the transfer process conserve linear and angular momentum—the so-called matching conditions. In addition, Brink assumes that the transfer is peripheral in nature, i.e., a grazing trajectory. Such conditions predict most-probable ejectile energies as shown in Fig. 28 for the 341-MeV ^{16}O+^{197}Au reaction. Also in Fig. 28, we have plotted the mean ejectile energies in our measured $S=0$ events. As can be seen, Brink's model does not reproduce the velocity damping of the light ejectiles.

The overlap model uses Brink's kinematic conditions but, in addition, requires that the transferred mass be contained in the spatial overlap of the projectile and target. This is quite different from the assumption of grazing trajectories and, when used in conjunction with the matching conditions, yields mean ejectile energies in better accord with experiment. In particular, the systematic variations of ejectile energy with A (for fixed Z) and with Z (for fixed A) are reproduced.

In order to analyze the experimental widths of the energy spectra, we need a model that can supply more detail than is obtained from the kinematic models considered so far. Such a model has been constructed by McVoy and
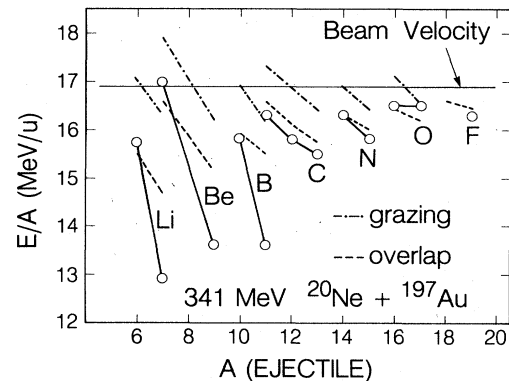

FIG. 28. The most-probable energies for $S=0$ ejectiles are plotted as a function of ejectile mass. Also shown are calculated energies (Ref. 29) using the Brink semiclassical matching conditions as applied to either overlap (dashed) or grazing (dot-dashed) geometries.

Nemes,[36] who utilize a local-momentum plane-wave Born approximation (LMPWBA) to predict the observed energy spectra of ejectiles produced in direct reactions. Their model is able to deal with transfer and sequential breakup as separate processes. [Specific calculations have been made only for the reaction ^{208}Pb(^{16}O,^{12}C) at 20 MeV/nucleon.]

In general, the LMPWBA predicts that the transfer spectra will possess larger means and smaller widths than the corresponding breakup spectra. The smaller width of the ejectile energy distribution when the lost charge is transferred to the target nucleus is understood in terms of phase space: the capture of mass by the target imposes a constraint that does not exist for breakup, resulting in a narrower distribution.

The measured $S=0$ and $S=1$ means and widths appear to be in qualitative agreement with the above prediction of McVoy and Nemes for the heaviest ejectiles, where the transfer events possess a larger mean and smaller width than the corresponding breakup spectra. However, for $Z<7$, the experimental widths for transfer become larger than for breakup, in disagreement with their prediction. In their analysis, however, McVoy and Nemes restrict their LMPWBA to small mass transfer, arguing that large mass transfer is probably mediated by a different, or additional, reaction mechanism.

Analyses of the energy spectra using other, more elaborate, direct-reaction models would be valuable. For example, a DWBA based on the diffraction model, as applied by Mermaz et al.,[37] would seem well suited for analysis of few-nucleon transfer, providing that the calculations be appropriately modified to take into account the low particle-decay thresholds of the relatively light projectilelike fragments encountered in this work. In particular, the $S=0$ energy spectra are well suited for comparison with a DWBA calculation since one knows that the spectra are uncontaminated by breakup processes. Furthermore, the excited states of the ejectile that must be included in the calculation are limited to a relatively few bound

states. A multistep extension of the DWBA, the breakup-fusion model of Udagawa and Tamura,[38,39] could be used for the larger mass transfers.

VI. SUMMARY

We have used a 4π charged particle detector, the Plastic Box, to measure the relative importance of transfer and breakup in 11- and 17-MeV/nucleon ^{20}Ne-induced reactions on ^{197}Au targets. At the lower energy, transfer is the main contributor to the inclusive ejectile yields. Surprisingly, transfer is still prominent at the higher bombarding energy, though breakup is now found to strongly influence the observed distribution of ejectile charge.

The relative amounts of transfer and breakup in inclusive ejectile yields were found to be rather insensitive to scattering angle at 341 MeV over the angular range $8°–21°$. At both bombarding energies, the inclusive fluorine yields were almost entirely due to charge transfer. The importance of breakup increased with decreasing ejectile charge, leveling off for $Z \leq 7$. In this region of massive charge transfer, pure transfer (i.e., $S = 0$) was responsible for $\simeq 60\%$ of the observed inclusive yield at 220 MeV, and $\simeq 30\%$ of the yield at 341 MeV.

In order to make comparisons with reaction models, the experimentally determined breakup cross sections were used to make reconstructions of the primary ejectile yields. It was found that at both 11 and 17 MeV/nucleon, the overlap[27] and sum-rule[28] models were able to reproduce most of the yields. However, for the lightest primary fragment (boron) there were substantial differences, with the sum-rule model more successful at the lower bombarding energy and the overlap model doing better at the higher energy. In making these comparisons, we have made the assumption (borne out by other experimental studies) that most, if not all, of the breakup yield is sequential rather than direct.

By calculating the fraction of the deduced primary yield that contributes to the inclusive cross section, we are able to calculate the survival fraction of the primary ejectile, i.e., the probability that the ejectile was produced in a bound state. The results indicate relatively large survival fractions even at 341 MeV, and at both energies the probability of sequential breakup is slowly changing over a large range of transferred mass and, hence, total excitation energy. This argues against an equal sharing of excitation energy in the primary system. Rather, the data are consistent with the target nucleus acquiring most of the excitation energy via a unidirectional mass flow.

At 341 MeV, the energy spectra of the various ejectiles were compared by extracting the first four central moments (mean, width, skewness, and kurtosis). For a given ejectile, the transfer and breakup energy spectra were found to be very similar. When combined with Brink's semiclassical matching conditions, the geometry of the overlap model yields[29] mean ejectile energies in good agreement with experiment. The experimental widths of the energy spectra for the heavier ejectiles are consistent with systematics predicted by McVoy and Nemes,[36] with transfer spectra being narrower (as well as more energetic) than breakup. The reversal of this trend for the lighter ejectiles is believed to signify the presence of competing processes.

*Present address: Department of Nuclear Physics, Weizmann Institute of Science, Rehovot 76100, Israel.

†Present address: Nuclear Physics Laboratory, University of Washington, Seattle, WA 98195.

[1]J. Blocki, Y. Boneh, J. R. Nix, J. Randrup, M. Robel, A. J. Sierk, and W. J. Swiatecki, Ann. Phys. (N.Y.) **113**, 338 (1978).

[2]J. W. Negele, Rev. Mod. Phys. **54**, 913 (1982).

[3]N. J. DiGiacomo and R. M. DeVries, Comments Nucl. Part. Phys. **12**, 111 (1984).

[4]D. K. Scott, Nucl. Phys. **A354**, 375c (1981).

[5]T. Nomura, H. Utsunomiya, T. Motobayashi, T. Inamura, and M. Yankura, Phys. Rev. Lett. **40**, 694 (1978).

[6]J. Wilczynski, K. Siwek-Wilczynska, J. van Driel, S. Gonggrijp, D. C. J. M. Hageman, R. V. F. Janssens, J. Lukasiak, and R. H. Siemssen, Phys. Rev. Lett. **45**, 606 (1980).

[7]D. R. Zolnowski, H. Yamada, S. E. Cala, A. C. Kahler, and T. T. Sugihara, Phys. Rev. Lett. **41**, 92 (1978).

[8]R. G. Stokstad, M. N. Namboodiri, E. T. Chulick, J. B. Natowitz, and D. L. Hanson, Phys. Rev. C **16**, 2249 (1977).

[9]A. C. Shotter, A. N. Bice, J. M. Wouters, W. D. Rae, and J. Cerny, Phys. Rev. Lett. **46**, 12 (1981).

[10]M. J. Murphy, S. Gil, M. N. Harakeh, A. Ray, A. G. Seamster, R. Vandenbosch, and T. C. Awes, Phys. Rev. Lett. **53**, 1543 (1984).

[11]U. Jahnke, G. Ingold, H. Homeyer, M. Burgel, Ch. Egelhaaf, H. Fuchs, and D. Hilscher, Phys. Rev. Lett. **50**, 1246 (1983).

[12]H. W. Wilschut, R. K. Bhowmik, P. B. Goldhoorn, J. F. W. Jansen, R. H. Siemssen, K. Siwek-Wilczynska, Z. Sujkowski, and J. Wilczynski, Phys. Lett. **123B**, 173 (1983).

[13]K. Van Bibber, W. Pang, M. Avery, and E. Bloemhof, IEEE Trans. Nucl. Sci. **NS-27**, 86 (1980).

[14]K. Van Bibber, P. J. Countryman, M. J. Murphy, Y. D. Chan, R. G. Stokstad, I. Tserruya, and S. Wald, IEEE Trans. Nucl. Sci. **NS-31**, 35 (1984).

[15]M. J. Murphy, B. G. Harvey, D. L. Hendrie, W. W. Pang, K. Van Bibber, and R. Legrain, Phys. Lett. **120B**, 75 (1983).

[16]M. Bini, C. K. Gelbke, D. K. Scott, T. J. M. Symons, P. Doll, D. L. Hendrie, J. L. Laville, J. Mahoney, M. C. Mermaz, C. Olmer, K. Van Bibber, and H. H. Wieman, Phys. Rev. C **22**, 1945 (1980).

[17]G. R. Young, R. L. Ferguson, A. Gavron, D. C. Hensley, F. E. Obenshain, F. Plasil, A. H. Snell, M. P. Webb, C. F. Maguire, and G. A. Petitt, Phys. Rev. Lett. **45**, 1389 (1980).

[18]A. Gamp, M. Burgel, M. R. Clover, C. Egelhaaf, H. Fuchs, B. Gebauer, H. Homeyer, and J. C. Jacmart, Z. Phys. A **300**, 63 (1981).

[19]S. Wald, I. Tserruya, Z. Fraenkel, G. Doukellis, H. Gemmeke, and H. L. Harney, Phys. Rev. C **25**, 1118 (1982).

[20]H. Homeyer, M. Burgel, M. Clover, Ch. Egelhaaf, H. Fuchs, A. Gamp, D. Kovar, and W. Rauch, Phys. Rev. C **26**, 1335 (1982).

[21]P. B. Goldhoorn, G. J. Balster, H. J. Koeslag, R. J. de Meijer, R. H. Siemssen, Z. Sujkowski, and H. W. Wilschut, Phys. Lett. **142B**, 14 (1984).

[22]M. Bantel, R. G. Stokstad, Y. D. Chan, S. Wald, and P. J. Countryman, Nucl. Instrum. Methods **226**, 394 (1984).

[23]M. Blann, ALERT, statistical-model code (unpublished).

[24]M. Hillman and Y. Eyal, JULIAN, Monte Carlo statistical-model code (unpublished), modified by A. Gavron to couple angular-momentum projections.

[25]Ch. Egelhaaf, M. Burgel, H. Fuchs, A. Gamp, H. Homeyer, D. Kovar, and W. Rauch, Nucl. Phys. **A405**, 397 (1983).

[26]C. R. Albiston, Y-d. Chan, S. B. Gazes, H. R. Schmidt, R. G. Stokstad, S. Wald, and P. J. Countryman, Bull. Amer. Phys. Soc. **29**, 1054 (1984).

[27]B. G. Harvey and H. Homeyer, submitted to Phys. Lett. B.

[28]J. Wilczynski, K. Siwek-Wilczynska, J. van Driel, S. Gong-grijp, D. C. J. M. Hageman, R. V. F. Janssens, J. Lukasiak, R. H. Siemssen, and S. Y. van der Werf, Nucl. Phys. **A373**, 109 (1982).

[29]B. G. Harvey and M. J. Murphy. Phys. Lett. **130B**, 373 (1983).

[30]J. Hufner, K. Schafer, and B. Schurmann, Phys. Rev. C **12**, 1888 (1975).

[31]W. A. Friedman, Phys. Rev. C **27**, 569 (1983).

[32]J. B. Natowitz, Proceedings of the International Conference on Nuclear Physics, Bombay, 1984.

[33]T. C. Awes, R. L. Ferguson, R. Novotny, F. E. Obenshain, F. Plasil, S. Pontoppidan, V. Rauch, G. R. Young, and H. Sann, Phys. Rev. Lett. **52**, 251 (1984).

[34]R. Vandenbosch, A. Lazzarini, D. Leach, D.-K. Lock, A. Ray, and A. Seamster, Phys. Rev. Lett. **52**, 1964 (1984).

[35]D. M. Brink, Phys. Lett. **40B**, 37 (1972).

[36]K. W. McVoy and M. C. Nemes, Z. Phys. A **295**, 177 (1980).

[37]M. C. Mermaz, J. Barrette, and H. E. Wegner, Phys. Rev. C **24**, 2148 (1981); M. C. Mermaz, F. Auger, and B. Fernandez, *ibid.* **28**, 1587 (1983).

[38]T. Udagawa and T. Tamura, Phys. Rev. Lett. **45**, 1311 (1980).

[39]T. Udagawa, D. Price, and T. Tamura, Phys. Lett. **116B**, 311 (1982).
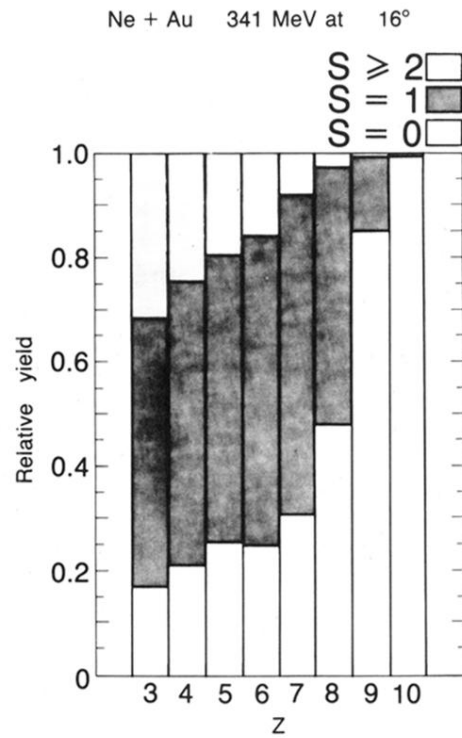
FIG. 3. The wall multiplicity, S, is plotted as a function of the charge of the trigger ejectile detected at 16°. The data are corrected for neutral events, but not for contributions from sequential target emission of charged particles.